Proceedings of The 19th International Conference on Solid State Ionics (SSI-19)

Submitted 11 May 2013

Revised 1 September 2013

Synthesis and properties of Al-free $Li_{7-x}La_3Zr_{2-x}Ta_xO_{12}$ garnet related oxides

Ryoji Inada*, Koji Kusakabe, Takayuki Tanaka, Shota Kudo, and Yoji Sakurai

Department of Electrical and Electronic Information Engineering, Toyohashi University of Technology, 1-1 Hibarigaoka, Tempaku-cho, Toyohashi, Aichi 441-8580, Japan.

*Corresponding author

Ryoji Inada, Associate Professor

Postal address: Toyohashi University of Technology, 1-1 Tempaku-cho, Toyohashi, Aichi 441-8580, Japan

Phone: +81-532-44-6723

Fax: +81-532-44-6757

E-mail address: inada@ee.tut.ac.jp

Abstract

We investigated the properties of Al-free garnet related $Li_7La_3Zr_2O_{12}$ (LLZ) and $Li_{7-x}La_3Zr_{2-x}Ta_xO_{12}$ (LLZTa) with Ta content x = 0.25, 0.5 and 1.0 synthesized by a solid state reaction method. It was confirmed that all Al-free LLZTa have the cubic garnet related structure, while Al-free LLZ without Ta substitution has tetragonal one. No other secondary phases were observed in all sintered samples. This indicates that partial substitution of Zr^{4+} by Ta^{5+} with higher valence increases Li-ion vacancy concentration in a garnet framework and stabilizes cubic garnet structure. The LLZTa grains are in good contact with each other although a certain amount of pores in the boundary area can be observed. Total (bulk + grain boundary) Li-ion conductivity at 27°C for all Al-free LLZTa were well above 10^{-4} Scm^{-1}, while Al-free LLZ showed much lower room temperature conductivity of 1×10^{-5} Scm^{-1}. The highest room temperature conductivity of 6.1×10^{-4} Scm^{-1} was obtained in Al-free LLZTa with x = 0.5, which is approximately 30–40% lower than the value in LLZTa (x = 0.5) with Al inclusion as previously reported.

Keywords: $Li_7La_3Zr_2O_{12}$ garnet, cubic structure, Al-free, Ta substitution, ionic conductivity

1. Introduction

All-solid-state Li-ion batteries are expected as one of the next generation energy stored devices because of their high energy density, high safety and excellent cycle stability [1]. Development of solid inorganic Li-ion conducting materials for the use as solid electrolyte is most important issue to realize all solid-state Li-ion batteries. The materials used for solid electrolyte must have not only high Li-ion conductivity $\sigma_{Li} > 10^{-3}$ Scm^{-1} at room temperature but also chemical stabilities against Li metal, air and moisture. Although oxide based solid electrolyte materials have rather lower σ_{Li} than sulfide based one [1], they have other advantages such as their chemical stability and handling.

Garnet related lithium stuffed oxides with the formula of $Li_7La_3Zr_2O_{12}$ (LLZ) have been widely studied because of their high Li-ion conductivity $\sigma_{Li} > 10^{-4}$ Scm^{-1} at room temperature, excellent thermal performance and stability against Li metal anode [2]. LLZ has two different crystal phases, one is cubic phase and another is tetragonal one [3–5]. Li-ion conductivity in cubic LLZ approximately two orders higher than tetragonal one, but sintering at high temperature around 1200°C for several 10 h is needed to obtain dense cubic LLZ [2]. High total (bulk + grain boundary) conductivity at room temperature above 10^{-4} Scm^{-1} is mostly confirmed in cubic LLZ sintered in alumina crucible and/or substituted Al_2O_3 [2, 6–9]. During the high temperature sintering, Al^{3+} enters from the crucible and/or substituted Al_2O_3 into LLZ pellet and works as sintering aid. In addition, it has been pointed out that some amount of Al^{3+} enters into LLZ lattice, modifies the Li-ion vacancy concentration in a garnet framework and stabilizes cubic structure [8, 9].

Recently, partial substitution of Zr by Nb [10] or Ta [11–13] in LLZ is reported to

be effective to stabilize the cubic garnet structure, and their total conductivity was greatly enhanced up to ~ 1×10^{-3} Scm^{-1} by optimizing the content of Nb and Ta [10, 11]. Such high conductivity is considered to be achieved by both the optimized Li-ion vacancy concentration in garnet framework by higher valence cation (Nb^{5+} or Ta^{5+}) doping and the densification by Al^{3+} entering from alumina crucible during high temperature sintering [11]. The former directly contributes to enhance bulk conductivity and the latter is considered to be effective to reduce grain boundary resistance. However, the possibility for achieving high total conductivity in Nb or Ta substituted LLZ without the help for Al inclusion has not been fully investigated.

In this study, we synthesized garnet related $Li_{7-x}La_3Zr_{2-x}Ta_xO_{12}$ (LLZTa) with different Ta content x under Al-free condition. Influence of Ta content on crystal phase formation, microstructure and ionic conductivity of Al-free LLZTa was investigated. In addition, the property of Al-free LLZTa was compared with LLZTa with Al inclusion as previously reported in [11].

2. Experimental

Al-free $Li_7La_3Zr_2O_{12}$ (LLZ) and $Li_{7-x}La_3Zr_{1-x}Ta_xO_{12}$ (LLZTa) oxides with different Ta content x = 0.25, 0.5 and 1 were prepared by a solid state reaction method. Stoichiometric amounts of Li_2CO_3 (10% excess was added to account for the evaporation of lithium at high temperatures), $La(OH)_3$, ZrO_2 and Ta_2O_5 were ground and mixed by planetary ball-milling (Nagao System, Planet M2-3F) with zirconia ball, and then calcined at 900°C for 6 h in Pt-Au5% alloy crucible. The calcined powders were ground again, and then pressed into pellets at 300 MPa by cold isostatic pressing (CIP). Finally, all LLZTa pellets were sintered at 1100°C for 15 h in air using Pt-Au5%

alloy crucible. The sintering condition for Al-free LLZTa was referred to that for LLZTa with Al inclusion from alumina crucible reported in [11]. At sintering stage, the pellet was covered with the same mother powder to suppress the excess Li loss and the formation of secondary phase such as $La_2Zr_2O_7$. Similar fabrication procedure was used for preparation of Al-free LLZ without Ta substitution but sintering temperature and time were set to 1200°C and 24 h. This sintering condition was optimized to obtain dense Al-free LLZ pellet. It is noted that Al-free LLZ could not be sintered successfully when sintering condition was set to 1100°C for 15h.

The crystal structure of the samples was evaluated by X-ray diffraction (XRD, Rigaku Multiflex) using CuKα radiation, with measurement range 2θ = 5–90° and step interval of 0.04°. Scanning electron microscope (SEM) and energy dispersive X-ray (EDX) analyses were performed using JSM-6300 (JEOL Ltd.) to investigate the fractured surface microstructure of the sintered pellet and the distribution of La, Zr and Ta elements. The composition of the elements in each sample was measured by inductively coupled plasma optical emission spectroscopy (ICP-OES). Ionic conductivity was evaluated at temperature from 27 to 130°C and frequency from 5 Hz to 5 MHz, with both Hioki Chemical Impedance Meter 3532-80 (for the measurement up to 1 MHz) and Hioki LCR Hightester 3532-50 (for the measurement from 1 MHz to 5 MHz). Both parallel surfaces of the pellet were sputtered with Li-ion blocking Au electrodes for the measurement.

3. Results and discussion

XRD patterns of Al-free $Li_7La_3Zr_2O_{12}$ (LLZ) and Al-free $Li_{7-x}La_3Zr_{2-x}Ta_xO_{12}$ (LLZTa) with different Ta content x = 0.25, 0.5 and 1.0 are summarized in Fig. 1.

Calculated peak patterns for both cubic and tetragonal LLZ are also shown for comparison [3, 4]. It can be confirmed that under applying synthesis conditions, Al-free LLZ without Ta substitution has a predominant tetragonal garnet related structure. On the other hand, all of the observed diffraction peaks Al-free LLZTa with x = 0.25–1 were well indexed as a cubic garnet related structure. No other secondary phases were observed in all samples. Partial substitution of Zr^{4+} by Ta^{5+} with higher valence increases Li-ion vacancy concentration in a garnet framework, which mainly contributes to stabilize cubic garnet structure. Comparing with the calculated peak patterns for cubic LLZ, all diffraction peaks of LLZTa are shifted toward higher angle 2θ and this tendency becomes more significant with increasing Ta content. This could be caused by change of lattice parameter for LLZTa depending on x. Similar results are also confirmed in Nb or Ta substituted LLZ with Al inclusion as previously reported [10–13]. Lattice size of LLZTa could be decreased with increasing x probably due to the substitution of larger Zr^{4+} (72 pm) by smaller Ta^{5+} (64 pm).

The density of each sintered pellet was determined from the weight and the physical dimensions. Measured and relative density (normalized by the theoretical density) of Al-free LLZTa with different Ta contents x and Al-free LLZ pellets are summarized in Table 1. Here, the theoretical density for each composition was calculated from the structural data described in [12]. The relative density of sintered LLZTa and LLZ pellets were estimated to be in the range between 89 and 92%, indicating that the difference in relative density among the pellets with different composition is small.

Fig. 2(a) shows fractured cross sectional SEM images of Al-free LLZTa with Ta content x = 0.5. Corresponding elementary mapping of La, Zr and Ta is also shown in

Fig. 2(b-d). It can be seen that all elements are uniformly distributed in the sample, indicating that Zr^{4+} are successfully substituted by Ta^{5+}. From ICP analysis, it was confirmed that the molar ratios of Li:La:Zr:Ta in Al-free LLZTa with different Ta content x = 0.25, 0.5 and 1 were be 6.82:3.0:1.75:0.25, 6.39:3.0:1.48:0.50 and 6.02:3.0:1.01:1.05, while the ratio of Li:La:Zr in Al-free LLZ was 7.08:3.0:1.9. The obtained molar ratios for all sintered samples are nearly corresponding to nominal compositions. We confirmed that Li^+ concentration in Al-free LLZTa decreases monotonically with increasing Ta content x and Al-free LLZ with tetragonal symmetry has the highest Li^+ concentration among the all samples.

Magnified SEM image of same sample is also shown in Fig. 3. Average grain size in the sintered pellet was confirmed to be 5 μm. LLZTa grains are in good contact with each other, but grain boundary is clearly visible and certain amount of small pores in the boundary area can be also observed. It is worth to note that the morphology of grain boundary of our Al-free LLZTa is different from LLZTa with Al inclusion reported in [11]. For LLZTa with Al inclusion, Al^{3+} entering from alumina crucible during high temperature sintering is predominantly distributed in grain boundary area and form amorphous phase by reacting with Li and O. This amorphous phase spreads effectively between the LLZTa grains and probably helps to improve connectivity among the grains.

The conductivity of Al-free LLZ and Al-free LLZTa with different Ta content x was examined by AC impedance spectroscopy using Li-ion blocking Au electrode. Fig. 3 shows typical impedance plots measured at room temperature (27°C) for all sample. For direct comparison among the samples with different geometrical sizes, real and imaginary parts of impedance *Z* and *Z*" multiplied by a factor of *A*/*l* are plotted in Fig. 4,

where A and l are surface area and thickness of each pellet. For all sample, semicircle and linear portion data were obtained in high and low frequency regions, indicating that the conducting nature is primary ionic. Only one semicircle was clearly confirmed, and the intercept point of linear tail in low frequency range with real axis corresponds to bulk and grain-boundary resistance. Total conductivity σ for each sample can be calculated by the inverse of bulk and grain boundary resistance. The values of σ at 27°C for all sample calculated from the data in Fig. 4 are summarized in Table 2. σ for all Al-free LLZTa with cubic symmetry was well above 10^{-4} Scm^{-1} and the highest $\sigma = 6.1 \times 10^{-4}$ Scm^{-1} was obtained in LLZTa with x = 0.5. On the other hand, Al-free LLZ with tetragonal symmetry showed much lower $\sigma \sim 1 \times 10^{-5}$ Scm^{-1}. This value is nearly comparable with the reported one for dense tetragonal LLZ with relative density of 98% prepared by hot pressing [14].

Temperature dependence of conductivity for all samples was also evaluated in the temperature range from 27 to 130°C. Fig. 5 shows variation of the conductivity σ for all sintered samples as a function of inverse of temperature 1000/T. Al-free LLZTa with Ta content x = 0.5 has the highest σ, while Al-free LLZ with tetragonal structure has the lowest one in the whole measurement range. The temperature dependence of σ is expressed by the Arrhenius equation as follows:

$$\sigma T = \sigma_0 \exp\left(-E_a / k_B T\right) \quad (1)$$

Here, σ_0 is constant, E_a is activation energy of conductivity and k_B is Boltzmann constant (= 1.381×10^{-23} J/K), respectively. As shown in (1), E_a of each sample can be estimated from the slope of σT data plotted in Fig. 5. As summarized in Table 2, activation energies E_a of Al-free LLZTa samples were estimated to be 0.40–0.42 eV.

As mentioned above, LLZ with tetragonal symmetry has higher content and local ordering of Li in a garnet framework [4, 5], and the bulk ionic conductivity for tetragonal symmetry is much lower than for cubic one. Moreover, total conductivity of polycrystalline material is also affected by grain-boundary resistance and grain boundary is closely related to relative density. Since the difference in relative density between LLZ and LLZTa pellets prepared in the present work is sufficiently small, the difference in total conductivity between Al-free LLZTa and Al-free LLZ in Fig. 5 and Table 2 is mainly attributed to the difference in bulk ionic conductivity of cubic and tetragonal symmetry.

Optimized Ta content x for LLZTa with Al inclusion has been reported to be 0.4–0.6 [11]. This is consistent with our results for Al-free LLZTa, but LLZTa with Al inclusion and optimized Ta content has higher room temperature conductivity $\sigma = 1 \times 10^{-3}$ Scm^{-1} and lower activation energy $E_a = 0.35$ eV than our Al-free sample [11]. As mentioned above, amorphous Li-Al-O phase at grain boundary area was formed in LLZTa with Al inclusion, which probably helps to improve connectivity among the LLZTa grains. On the other hand, such amorphous phase could not be confirmed in our Al-free LLZTa, so that grain boundary resistance of Al-free LLZTa could be larger than that for LLZTa with Al inclusion. Moreover, bulk conductivity of LLZTa could be changed with structural and compositional displacement by Al-doping. Unfortunately, quantitative evaluation of the bulk and grain conductivity of Al-free LLZTa is insufficient at present, because the frequency range for our experimental set-up for AC impedance measurement is limited below 5 MHz. Difference in AC impedance at higher frequency range (~ several 10 MHz) should be examined further to clarify the influence of Al inclusion on both bulk and grain boundary conductivity of LLZTa.

4. Conclusion

Al-free garnet related $Li_7La_3Zr_2O_{12}$ (LLZ) and $Li_{7-x}La_3Zr_{2-x}Ta_xO_{12}$ (LLZTa) with Ta content x = 0.25, 0.5 and 1.0 were prepared by a solid state reaction method and their properties were investigated. All Al-free LLZTa have the cubic garnet related structure, while Al-free LLZ without Ta doping has tetragonal one. Total (bulk + grain boundary) Li-ion conductivity at 27°C for all Al-free LLZTa with x = 0.25, 0.5 and 1.0 were well above 10^{-4} Scm^{-1}, while Al-free LLZ with a tetragonal structure showed much lower conductivity of 1×10^{-5} Scm^{-1}. The highest room temperature conductivity of 6.1×10^{-4} Scm^{-1} was obtained in Al-free LLZTa with x = 0.5, which is approximately 30–40% lower than the value in LLZTa (x = 0.5) with Al inclusion as previously reported. The lower conductivity of Al-free LLZTa may caused by lower sinterability and higher grain boundary resistance than LLZTa with Al inclusion.

Acknowledgements

This work was partly supported by Research Grant (General Research) from TEPCO Memorial Foundation.

References

[1] K. Takada, Acta Mater. **61** (2013) 759–770.

[2] R. Murugan, V. Thangadurai, W. Weppner, Angew. Chem. Int. Ed. **46** (2007) 7778–7781.

[3] J. Awaka, N. Kijima, H. Hayakawa, J. Akimoto, J. Solid State Chem. **182** (2012) 2046–2052.

[4] J. Awaka, A. Takashima, K. Kataoka, N. Kijima, Y. Idemoto, J. Akimoto, Chem. Lett. **40** (2011) 60–62.

[5] C. A. Geiger, E. Alekseev, B. Lazic, M. Fisch, T. Armbruster, R. Langner, M. Fechtelkord, N. Kim, T. Pettke, W. Weppner, Inorg. Chem. **50** (2011) 1089–1097.

[6] M. Kotobuki, K. Kanamura, Y. Sato, T. Yoshida, J. Power Sources **196** (2011) 7750–7754.

[7] S. Kumazaki, Y. Iriyama, K.H. Kim, R. Murugan, K. Tanabe, K. Yamamoto, T. Hirayama, Z. Ogumi, Electrochem. Commun. **13** (2011) 509–512.

[8] E. Rangasamy, J. Wolfenstein, J. Sakamoto, Solid State Ionics **206** (2012) 28–32.

[9] Y. Li, J. Han, C. Wang, S. C. Vogel, H. Xie, M. Xu, J.B. Goodenough, J. Power Sources **209** (2012) 278-281.

[10] S. Ohta, T. Kobayashi, J. Power Sources **196** (2011) 3342–3345.

[11] Y. Li, J. Han, C. Wang H. Xie, J.B. Goodenough, J. Mater. Chem. **22** (2012) 15357–15361.

[12] A. Logéat, T. Köhler, U. Eisele, B. Stiaszny, A. Harzer, M. Tovar, A. Senyshyn, H. Ehrenberg, B. Kozinsky, Solid State Ionics **206** (2012) 33–38.

[13] H. Buschmann, S Berendts, B. Mogwitz, J. Janek, Journal of Power Sources **206** (2012) 236–244.

[14] J. Wolfenstein, E. Rangasamy, J.L. Allen, J. Sakamoto, Journal of Power Sources **208** (2012) 193–196.

Table 1. Measured, theoretical and relative density of Al-free $Li_7La_3Zr_2O_{12}$ and Al-free $Li_{7-x}La_3Zr_{2-x}Ta_xO_{12}$ with Ta content x = 0.25, 0.5 and 1.0. Note that theoretical density for each composition was determined by using data in [12].

Sample composition	Measured density (g cm^{-3})	Theoretical density (g cm^{-3})	Relative density (%)
$Li_7La_3Zr_2O_{12}$	4.64	5.11	91
$Li_{6.75}La_3Zr_{1.75}Ta_{0.25}O_{12}$ (x = 0.25)	4.82	5.21	92
$Li_{6.5}La_3Zr_{1.5}Ta_{0.5}O_{12}$ (x = 0.5)	4.80	5.31	89
$Li_6La_3ZrTaO_{12}$ (x = 1.0)	5.07	5.51	92

Table 2. Total conductivity σ at 27°C and activation energy E_a of Al-free $Li_7La_3Zr_2O_{12}$ and Al-free $Li_{7-x}La_3Zr_{2-x}Ta_xO_{12}$ with Ta content x = 0.25, 0.5 and 1.0.

Sample composition	σ (Scm^{-1}) at 27°C	E_a (eV)
$Li_7La_3Zr_2O_{12}$ (Tetragonal)	9.9×10^{-6}	0.43
$Li_{6.75}La_3Zr_{1.75}Ta_{0.25}O_{12}$ (x = 0.25, Cubic)	4.1×10^{-4}	0.42
$Li_{6.5}La_3Zr_{1.5}Ta_{0.5}O_{12}$ (x = 0.5, Cubic)	6.1×10^{-4}	0.40
$Li_6La_3ZrTaO_{12}$ (x = 1.0, Cubic)	2.1×10^{-4}	0.42

Figure captions

Fig. 1. XRD patterns of Al-free $Li_7La_3Zr_2O_{12}$ (LLZ) and Al-free $Li_{7-x}La_3Zr_{2-x}Ta_xO_{12}$ (LLZTa) with different Ta content x: (a) LLZTa with x = 0.25, (b) LLZTa with x = 0.5, (c) LLZTa with x = 1.0 and (d) LLZ.

Fig. 2. SEM image of the fractured cross section for Al-free $Li_{7-x}La_3Zr_{2-x}Ta_xO_{12}$ with Ta content x = 0.5 (a) and corresponding mapping of La (b), Zr (c) and Ta (d) obtained from EDX analysis.

Fig. 3. Magnified SEM image of the fractured cross section for Al-free $Li_{7-x}La_3Zr_{2-x}Ta_xO_{12}$ with Ta content x = 0.5

Fig. 4. AC impedance plot obtained at 27°C for (a) Al-free $Li_7La_3Zr_2O_{12}$ (LLZ) and (b) Al-free $Li_{7-x}La_3Zr_{2-x}Ta_xO_{12}$ (LLZTa) with different Ta content x.

Fig. 5. Arrhenius plots for total (bulk + grain-boundary) ionic conductivity for $Li_7La_3Zr_2O_{12}$ (LLZ) and $Li_{7-x}La_3Zr_{2-x}Ta_xO_{12}$ (LLZTa) with different Ta content x = 0.25, 0.5 and 1.0.

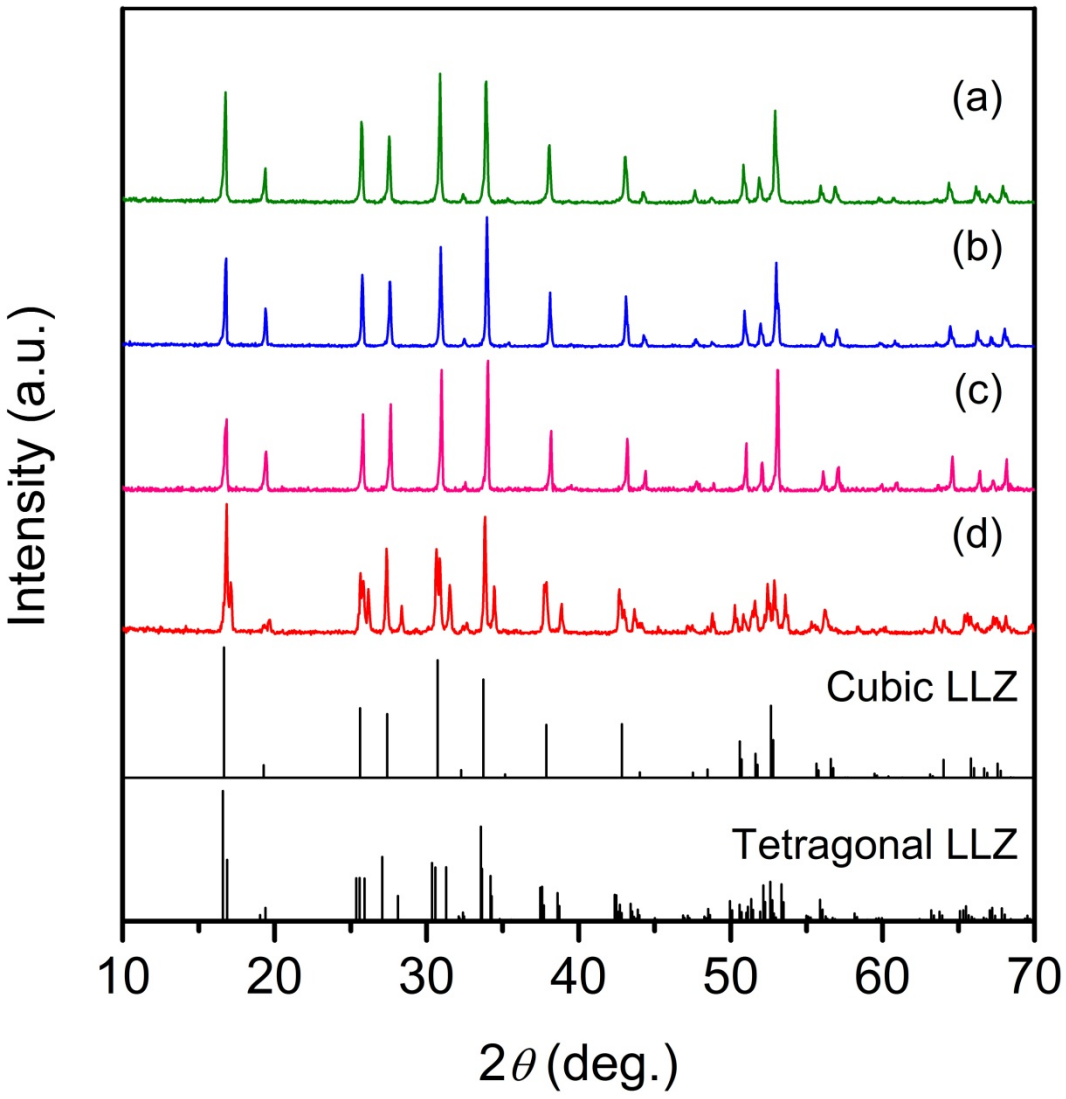
(a)
(b)
(c)
(d)
Cubic LLZ
Tetragonal LLZ
Intensity (a.u.)
10
20
30
40
50
60
70
2θ (deg.)

Fig. 1

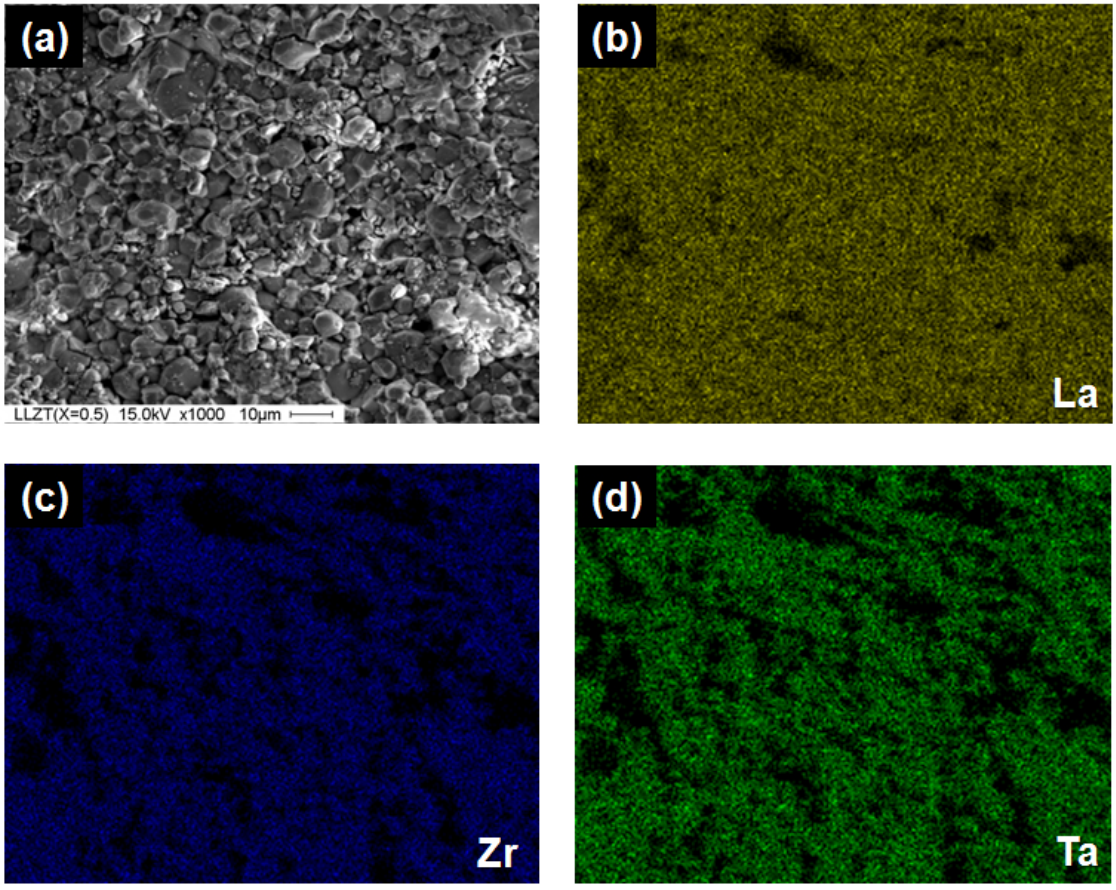

Fig. 2

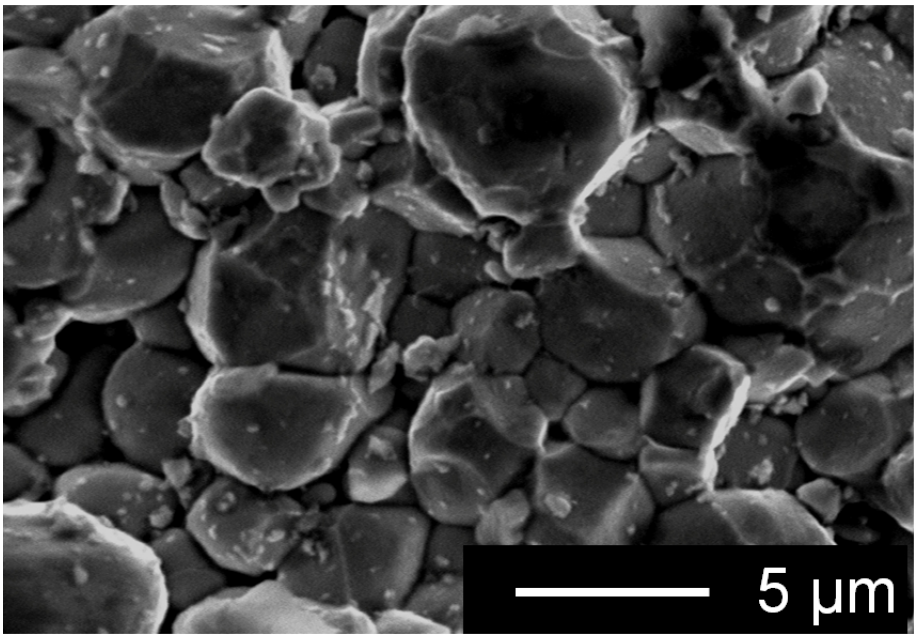

Fig. 3

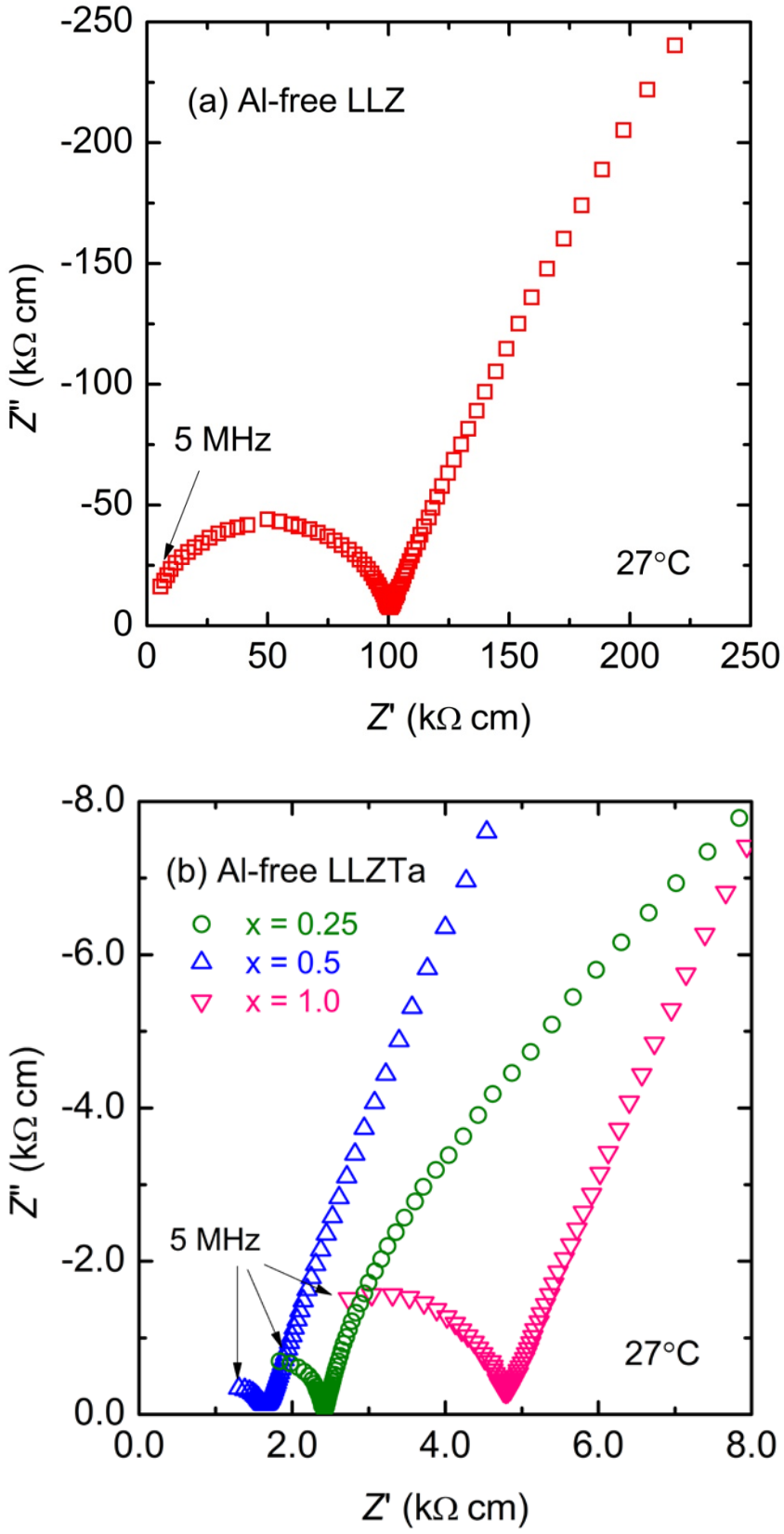
(a) Al-free LLZ
5 MHz
27°C
Z'' (kΩ cm)
Z' (kΩ cm)
-250
-200
-150
-100
-50
0
0
50
100
150
200
250
(b) Al-free LLZTa
x = 0.25
x = 0.5
x = 1.0
5 MHz
27°C
Z'' (kΩ cm)
Z' (kΩ cm)
-8.0
-6.0
-4.0
-2.0
0.0
0.0
2.0
4.0
6.0
8.0

Fig. 4

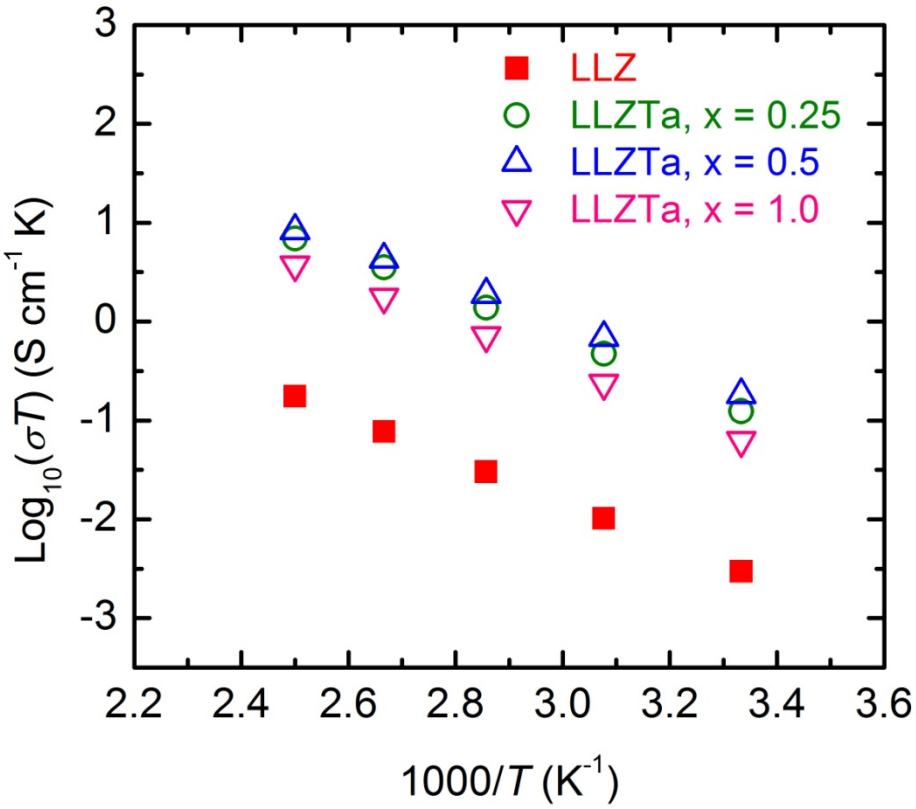
LLZ
LLZTa, x = 0.25
LLZTa, x = 0.5
LLZTa, x = 1.0
Log10(σT) (S cm-1 K)
1000/T (K-1)
3
2
1
0
-1
-2
-3
2.2
2.4
2.6
2.8
3.0
3.2
3.4
3.6

Fig. 5